A Comprehensive Inertial Control Strategy for Hybrid AC/DC Microgrid with Distributed Generations

He, Li; Li, Yong; Guerrero, Josep M.; Cao, Yijia

Published in:
IEEE Transactions on Smart Grid

DOI (link to publication from Publisher):
10.1109/TSG.2019.2942736

Publication date:
2020

Document Version
Accepted author manuscript, peer reviewed version

This article has been accepted for publication in a future issue of this journal, but has not been fully edited. Content may change prior to final publication. Citation information: DOI 10.1109/TSG.2019.2942736, IEEE Transactions on Smart Grid

A Comprehensive Inertial Control Strategy for Hybrid AC/DC Microgrid with Distributed Generations

Li He, *Student Member, IEEE*, Yong Li, *Senior Member, IEEE*, Josep M. Guerrero, *Fellow, IEEE*, and Yijia Cao, *Senior Member, IEEE*

***Abstract*—Lack of inertia is one problem urgent for the stability of hybrid ac/dc system. In this paper, a comprehensive inertial control strategy is proposed for stability improvement of the hybrid ac/dc microgrid. The unified inertia index is introduced to evaluate the holistic inertia level of the hybrid microgrid. Besides, the coupling relationship between ac and dc nanogrid is discussed based on the power balance, which serves as the base of mutual inertial support. The characteristics of distributed generations (DGs) are analyzed, based on which the comprehensive inertial support is designed for various DGs respectively and adaptively divided into two responses: the local support and the cross-grid support. The proposed strategy takes full use of the rotational kinetic energy of wind turbine generator (WTG), and exploits the power capacity of distributed hybrid energy storages (HESs), which improves the global stability and dynamic performance of the hybrid microgrid during power disturbance. The performance of the proposed control strategy is validated by the simulation cases with different operating scenarios.**

***Index Terms*—Inertial control; hybrid ac/dc microgrid; distributed generations (DGs); wind turbine generator (WTG), hybrid energy storage (HES).**

NOMENCLATURE

RESs	Renewable energy sources.
IC	Interlink converter.
SG	Synchronous generator.
VSG	Virtual synchronous generator.
DGs	Distributed generations.
VIE	Virtual inertia emulation.
ES	Energy storage.
SC	Super-capacitor.
WTG	Wind turbine generator.
HES	Hybrid energy storage.
MTG	Micro-turbine generator.
PV	Photovoltaic.
PCC	Point of common coupling.
H_{ac}	Inertia of ac system.
J_i	Moment inertia of the i^{th} rotational device.
ω	Angular velocity.
f	Real-time frequency.
$S^i_{ac,N}$	Rated capacity of the i^{th} device in ac system.
P_f	Number of filed poles of SG.
H_{dc}	Inertia of dc system.
C^j_{dc}	Equivalent capacitance of the j^{th} device in dc System.
$V_{dc,j}$	DC voltage of the j^{th} device.
$S^j_{dc,N}$	Rated capacity of the j^{th} device in dc system.
H_u	Unified inertia.
f_0	Reference frequency.
V_{ref}	Reference dc voltage.
H_{VSG}	Correlation inertial constant.
C_{VC}	Correlation capacitance.
S_{IC}	Rated capacity of the IC.
MPPT	Maximum power point track.
STIS	Short-term inertial support.
$P^{\text{MPPT}}_{\text{PV}}$	Output power of PV with MPPT mode.
k^{dc}_{PV}	PV' s droop coefficients in dc side.
k^{ac}_{PV}	PV' s droop coefficients in ac side.
$f_{\max}$	Allowable maximum frequency.
$V^{\max}_{dc}$	Allowable maximum dc voltage.
ω_r	Mechanical rotor speed.
$H^{\text{STIS}}_{\text{WTG}}$	Equivalent inertia constant of WTG for STIS.
J_W	Moment of inertia of WTG.
ω_{MPPT}	Stable rotor speed of WTG in MPPT mode.
$\Delta P^{\text{STIS}}_{\text{WTG}}$	Increasing power of WTG for STIS.
Δt	Duration time of STIS.
k_{ES}	Proportional coefficient of HES for WTG-HES combined system.
$H^{\text{STIS}}_{\text{W\_E}}$	Inertial constant for the WTG-HES combined system for STIS.
$\Delta P^{\text{STIS}}_{\text{W\_ES}}$	Increasing power of the WTG-HES combined system for STIS.
k^{WTG}_{ac}	WTG's droop coefficient of ac side.
k^{WTG}_{dc}	WTG's droop coefficient of dc side.
$\Delta P^{\text{HES}}_{\text{LS}}$	Local inertial support power of HESs.
k^{HES}_{ac}	HES's droop coefficients of ac side.
k^{HES}_{dc}	HES's droop coefficients of dc side.
H^{ES}_{vir}	Virtual inertial constant of HES.
C^{ES}_{vir}	Virtual capacitance of HES.
T	Time constant of the filter.
k_c	Coupling coefficient of f and V_{dc}.
Δf_{vir}	Virtual frequency variation.
ΔV_{vir}	Virtual voltage variation.
ΔP_{IC}	Power reference of IC.

This work was supported in part by the Key Research and Development Program of Hunan Province of China under Grant 2018GK2031, in part by the national Natural Science Foundation of China (NSFC) under Grant 51822702, and in part by the Excellent Innovation Youth Program of Changsha of China under Grant KQ1802029. (Corresponding author: Y. Li)

L. He, Y. Li, and Y. Cao are with the College of Electrical and Information Engineering, Hunan University, Changsha 410082, China. (e-mail: helifamily@foxmail.com, yongli@hnu.edu.cn, and yjcao@hnu.edu.cn).

J. M. Guerrero is with the Department of Energy Technology, Aalborg University, 9220 Aalborg East, Denmark (e-mail: joz@et.aau.dk).

This article has been accepted for publication in a future issue of this journal, but has not been fully edited. Content may change prior to final publication. Citation information: DOI 10.1109/TSG.2019.2942736, IEEE Transactions on Smart Grid

I. Introduction

THE development of hybrid ac/dc microgrids has attracted much attention in academic and practical fields in recent years. The hybrid microgrid has many advantages such as less power conversion stages, friendly access for renewable energy sources (RESs), which will be the developing trend of the low-voltage power system [1]-[3]. However, there are also some issues for the hybrid structure. Firstly, the power sharing between ac and dc sections is crucial to maintain the power balance and enhance system stability. Thus the flexible control for interlink converter (IC) between the ac and the dc sides plays an important role for system operation and needs careful design. Secondly, the lack of inertia is one problem threatening the stability of ac or dc microgrid [4]-[6], which is also the key to be considered for hybrid microgrid's operation.

The IC can serve as a bridge transferring power between the ac and dc grids of the hybrid system. At present, there are two main control manners for the IC operation, i.e., communication based control and droop based control [7]. The centralized control is a typical communication based control strategy [8], [9], which uses a high functioning central controller to process the large amount of data transferred by communication network, and then the optimized power assignment signal is sent to IC to maintain power balance. An alternative method is the distributed control, which features neighboring information exchange and no central controller is required [10]. The precise and optimized power allocation can be achieved by communication based control. However, the reliability of the whole system is easily deteriorated during the communication failure, and the control performance highly depends on the power prediction accuracy.

The droop based control is also implemented in hybrid microgrid, which enjoys the advantage of no need of communication and acquires high reliability. In [11], a normalized operation is proposed to unify the scale of ac frequency and dc voltage, and then the developed *V-f-P* droop control can be obtained since the hybrid system can be regarded as a single microgrid. There are a few researches developed from this normalization droop method, which feature simple way to connect the ac and the dc grids and more comprehensive control strategy can be derived based on it [12]-[14]. The power sharing between ac and dc grids can be properly achieved by the normalized droop method. However, the dynamic performance, related to the inertia, is difficult to improve by only droop control.

Inertia is a crucial parameter to evaluate the stability of power system [15]. Due to the lack of rotational synchronous generator (SG), the inertial deficit problem is intrinsically threatening microgrid's operation. For the ac microgrid, to emulate inertial effect, the virtual synchronous generator (VSG) technique is proposed to help inverter behave like the real SG, which relies on the controllability and fast-speed response of power electronics, and requires that the connected distributed generations (DGs) have certain amount of power reserve capacity [16], [17]. Besides, the proper dispatch of various sources power can contribute to the system stability. In [18], a decentralized method is proposed to improve the frequency stability, which takes full use of power regulation ability of various DGs by detailed classification of microgrid's operational states. Some heuristic methods are also implemented for the load frequency control of ac microgrid, which can achieve a good control performance but easily be influenced by the system model precision [19], [20]. For the dc microgrid, the important key for the system stability is the dc bus voltage, and several researches have been conducted to maintain the voltage magnitude during power variation such as improved droop control [21], [22], hierarchical control [23], intelligent algorithm based control [24]. In the regard of transient dynamics of dc voltage, the virtual inertia emulation (VIE) is recently introduced to improve the dynamic behavior of dc voltage and can be extended in further research [25]. Compared with the sole ac or dc microgrid, the enhancement of system inertia for hybrid microgrid plays a more important role to maintain the system stability and improve the operation performance during power fluctuation, since the hybrid structure is more complicated. However, there are few researches conducted on this issue.

Since the energy storage (ES) can provide active power support besides suppressing RESs fluctuation, it is appropriate for inertial support [26]. In [27], a primary control strategy is proposed for the frequency and voltage regulation of MW microgrid, which uses the fast response feature of ES and can realize a tradeoff between droop deviation and transient performance. To make full use of advantages of different ES devices, i.e., high energy density of battery ES and high power density of super-capacitor (SC), adaptive control methods are performed in [28], [29], which all aim at better improving the microgrid's operational stability. Furthermore, the DG which processes rotary elements, e.g., wind turbine generator (WTG), can be involved in the inertial support. But the releasing kinetic energy should be designed to avoid WTG's halt or second power disturbance after releasing inertia [30]-[32].

In order to take full advantage of various DGs' inertial support capacity, a comprehensive control strategy is proposed in this paper, aiming at improving the holistic inertia level and operational performance of the entire hybrid microgrid. The contributions are summarized as follows:

1) The unified inertia index is defined to evaluate the holistic inertia level of the hybrid microgrid. The coupling relationship between ac and dc nanogrid is expressed based on the power balance and characteristics of both VSG and dc capacitor, which serves as the base of mutual inertial support power of the comprehensive strategy.
2) Based on the characteristics of DGs, the comprehensive inertial support is designed for various DGs. More specifically, the power ramp differences of different ES units and WTG's operating features are taken into consideration. Thus the proposed strategy can utilize the advantages of hybrid ES (HES) and WTG's inertial support capability, achieve reasonable power assignment between HES components, and improve the robustness of microgrid during power disturbance.
3) The proposed method is feasible to be implemented in

This article has been accepted for publication in a future issue of this journal, but has not been fully edited. Content may change prior to final publication. Citation information: DOI 10.1109/TSG.2019.2942736, IEEE Transactions on Smart Grid

practice, since it is derived from the developed droop principle and common converter control structures. As long as the original control structure of DG has the conventional droop control block, the implementation of the proposed method can be conveniently performed by modifying certain droop coefficient block. So it will not require complicated modification on the original controller and is convenient for practical use.

II. Characteristics of Unified Inertia and Coupling Relationship of Hybrid AC/DC Microgrid

Fig. 1 shows a general structure of hybrid ac/dc microgrid. As can be seen, the ac side is consisted of micro-turbine generator (MTG), WTG, HES unit and ac power loads. Similarly, the dc side comprises the photovoltaic (PV) panels, HES unit and typical dc loads. Both sides are connected through ICs. It should be noted that, without losing generality and ensuring the proposed strategy can be used for most scenarios, the elements in both sides are deployed in a symmetrical manner. Hence, the equipment in dotted boxes may be not in the corresponding nanogrid for reducing power conversion loss. The hybrid microgrid can be connected to the utility grid through the point of common coupling (PCC) in the ac side as required.

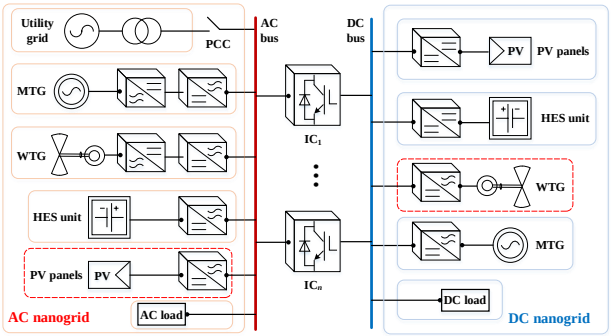

Fig. 1. General structure of the hybrid ac/dc microgrid.

A. Definition of Unified Inertia

The inertia of conventional ac power grid reflects the capability of damping the frequency change, which is provided by the SG and can be defined as [15]:

$$H_{ac}=\frac{\sum_{i=1}^{n}\frac{1}{2}J_i\omega^2}{\sum_{i=1}^{n}S_{ac,N}^{i}}=\frac{\sum_{i=1}^{n}2J_i\pi^2 f^2}{p_f^2\sum_{i=1}^{n}S_{ac,N}^{i}} \tag{1}$$

where J_i is the moment inertia of the i^{th} rotational device which is directly connected to the ac bus; ω is the angular velocity; f is the real-time frequency; and $S_{ac,N}^{i}$ is the rated capacity of the i^{th} device; P_f is the number of filed poles of SG. It is worth noting that if there are some DGs with rotary elements, connected into ac grid through power electronics (e.g. WTG with back-to-back converters), these DGs' inertia cannot be included in (1). More specifically, their rotor speed is decoupled from system frequency due to the converter control, and thus moment inertia cannot be directly used like SG, so their moment inertia cannot reflect the natural inertial level of ac grid and will not be included.

Similarly, the inertia of dc grid is introduced to reflect the ability of damping voltage variation, which is described as [33]

$$H_{dc}=\frac{\sum_{j=1}^{m}\frac{1}{2}C_{dc}^{j}V_{dc,j}^{2}}{\sum_{j=1}^{m}S_{dc,N}^{j}} \tag{2}$$

where C_{dc}^{j} is the equivalent capacitance of the j^{th} device; $V_{dc,j}$ is the dc voltage of the j^{th} device; $S_{dc,N}^{j}$ is the rated capacity of the j^{th} device. It is worth noting that, the device capacitance refers to the parallel physical capacitance near the dc bus. Although C_{dc}^{j} cannot be changed during operation, the dc voltage variation can still be reduced with certain control method by regulating power generation of some DGs, which also contributes to the improvement of H_{dc} stability.

To estimate the overall inertia of the hybrid ac/dc network, the unified inertia constant is defined here based on the total energy stored in the hybrid system divided by the capacity base. More specifically, the inertial constants of individual ac or dc part are normalized and combined to illustrate the unified inertia, which can effectively reflect the stability contribution of dc part, since the inertia of dc grid, determined by dc capacitor and usually with the unit of millisecond, is too small compared with that of ac grid. Therefore, the unified inertia, denoted as H_u, can be defined as:

$$H_u=H_{ac}\cdot\frac{\sum_{i=1}^{n}S_{ac,N}^{i}+\sum_{j=1}^{m}S_{dc,N}^{j}}{\sum_{i=1}^{n}\frac{2J_i\pi^2 f_0^2}{p_f^2}}+H_{dc}\cdot\frac{\sum_{i=1}^{n}S_{ac,N}^{i}+\sum_{j=1}^{m}S_{dc,N}^{j}}{\sum_{j=1}^{m}\frac{1}{2}C_{dc}^{j}V_{ref}^{2}} \tag{3}$$

where f_0 and V_{ref} are the reference frequency and the reference dc voltage, respectively.

The characteristics of H_u is depicted in Fig. 2. As can be seen, the value of H_u is enhanced by the increment of both dc voltage and ac frequency. It is worth noting that, even under the operation of normalization, the dc voltage change can contribute more to the inertia increase in allowable regions (corresponding to the variations within ±5% V_{ref} and ±1% f_0), resulting in the fast increase of H_u, which is illustrated by the slope variation trend of H_u when changing V_{dc} and f respectively, and also reflected by the difference of values of points B (H_u=4.165 s, f=49.5 Hz) and C (H_u=3.845 s, V_{dc}=627 V). In this paper, when the hybrid network operates in allowable regions, the proposed flexible control strategy will be activated to ensure smaller deviation from the rated operational point, which is discussed in Sec. III.

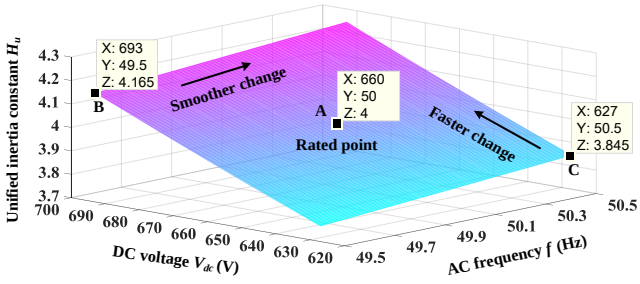

Fig. 2. Characteristics of the unified inertia in hybrid network (settings: V_{ref}=660 V, f_0=50 Hz, rated capacity of the hybrid system: 1 MVA)

This article has been accepted for publication in a future issue of this journal, but has not been fully edited. Content may change prior to final publication. Citation information: DOI 10.1109/TSG.2019.2942736, IEEE Transactions on Smart Grid

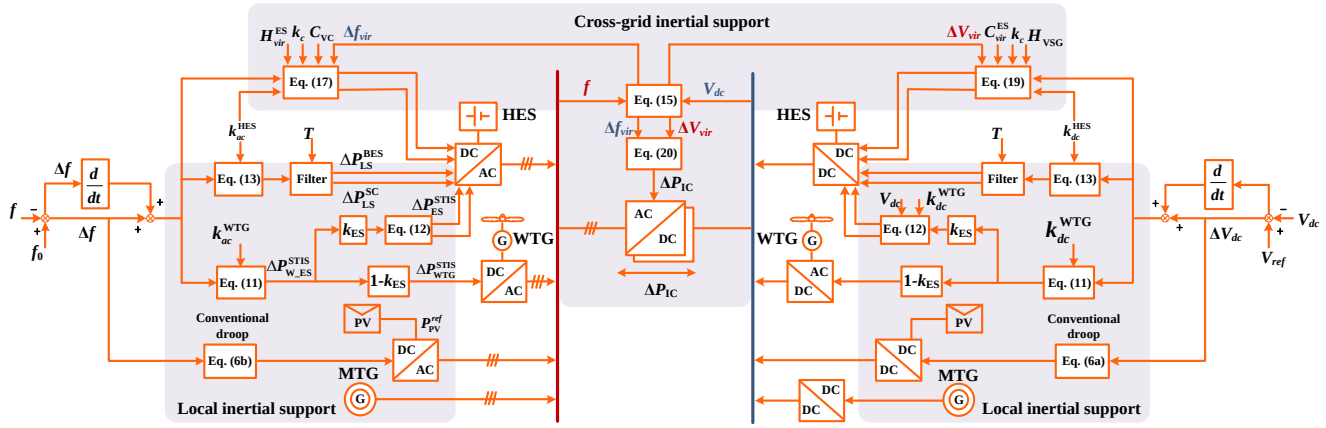

Fig. 4 Controller configuration of the proposed strategy for DGs and IC

B. Coupling Relationship of AC/DC Microgrid

The IC of the ac/dc interface can provide the bi-directional power support for the nanogrids. When the IC operates as an inverter, it offers frequency support for ac side and absorbs active power for dc capacitor of dc grid, which can be seen as a virtual synchronous generator. While the IC works as a rectifier, it can provide dc voltage support and can be seen as a virtual capacitor. Therefore, in the sense of active power balance, the coupling relationship between f and V_{dc} can be established with the coefficients of correlation inertia and capacitance, which is described as [34], [35]

$$\frac{C_{\mathrm{VC}}V_{dc}}{S_{\mathrm{IC}}}\frac{\mathrm{d}V_{dc}}{\mathrm{d}t}=\frac{2H_{\mathrm{VSG}}}{f_0}\frac{\mathrm{d}f}{\mathrm{d}t} \tag{4}$$

where H_{VSG} and C_{VC} are the correlation inertial constant and the correlation capacitance, respectively; and S_{IC} is the rated capacity of the IC.

Substituting V_{ref} -V_{dc} = ΔV_{dc} and f_0 - f =Δf into (4) yields

$$H_{\mathrm{VSG}}=\frac{C_{\mathrm{VC}}V_{ref}^2 f_0[1-(\frac{\Delta V_{dc}}{V_{ref}}-1)^2]}{4S_{\mathrm{IC}}\Delta f} \tag{5}$$

Fig. 3 gives an illustration of the relationship. It can be observed that, with the fixed value of C_{VC}, the increase of ΔV_{dc} will result in larger H_{VSG}, which means more power is absorbed from dc grid to improve the inertia of ac grid. In contrast, the increase of frequency deviation (corresponding to larger Δf) will bring opposite effect on H_{VSG}. In practice, the value of C_{VC} is determined according to the equivalent capacitance of dc grid, and then the value of H_{VSG} can be adjusted based on (5), which varies within the allowable deviation of frequency and dc voltage.

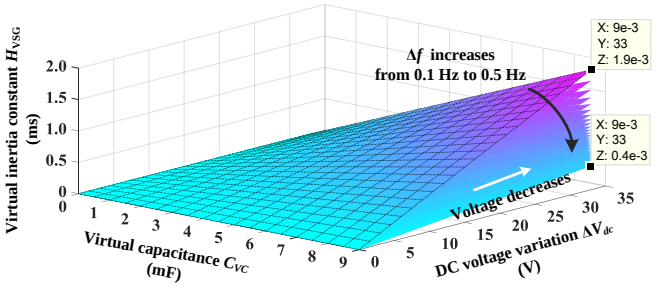

Fig. 3. Relationship between virtual inertial constant H_{VSG} and virtual capacitance C_{VC}

III. Comprehensive Flexible Control Strategy

A. Principles of the Strategy

Fig. 4 shows the comprehensive controller configuration block. Since the characteristics of various DGs are different from each other, the control strategy should be elaborated for different DGs respectively, of which the principles are illustrated as follows.

1) *PV panels:* Since PV panels generally work with maximum power point track (MPPT) mode [36], [37], they have no power margin available when the system requires more power. Therefore, the additional power management for PV generation can be activated when there is net power surplus.

2) *MTG*: It is usually operated as a back-up source or auxiliary service. MTG should be activated when the power deficiency cannot be compensated by other DGs, and it has no ability to respond to net power surplus.

3) *WTG*: The WTG possesses rotational element which provides short-term inertial support (STIS), but it will slow down the rotor speed and may cause the rotor's halt. Thus the HES unit, which is used to reduce the wind power fluctuation, can also be assigned to assist the inertial support and maintain the WTG's operating stability.

4) *HES*: The HES is an important element to track the net power variation and maintain the power balance. Due to its good controllability and fast response speed, the majority of inertial support power should be obtained from HES.

5) *IC*: This converter serves as the bridge of power transmission between two nanogrids, of which the control should be coordinated with the two sides' power states.

B. Control of PV Panels and MTG.

PV panels usually operate with MPPT mode to make full use of photovoltaic power. Thus it cannot increase output power to respond to the power deficit, and the conventional droop control method can only be applied when the generation reduction is required, as the following described

$$P_{\mathrm{PV}}^{ref}=k_{\mathrm{PV}}^{dc}(V_{ref}-V_{dc})+P_{\mathrm{PV}}^{\mathrm{MPPT}} \tag{6a}$$

$$P_{\mathrm{PV}}^{ref}=k_{\mathrm{PV}}^{ac}(f_0-f)+P_{\mathrm{PV}}^{\mathrm{MPPT}} \tag{6b}$$

where

This article has been accepted for publication in a future issue of this journal, but has not been fully edited. Content may change prior to final publication. Citation information: DOI 10.1109/TSG.2019.2942736, IEEE Transactions on Smart Grid

$$k_{\mathrm{PV}}^{dc}=\begin{cases}\dfrac{P_{\mathrm{PV}}^{\mathrm{MPPT}}}{V_{dc}^{\max}-V_{ref}}, & V_{dc}\geq V_{ref}\\ 0, & V_{dc}<V_{ref}\end{cases},\quad k_{\mathrm{PV}}^{ac}=\begin{cases}\dfrac{P_{\mathrm{PV}}^{\mathrm{MPPT}}}{f_{\max}-f_0}, & f\geq f_0\\ 0, & f<f_0\end{cases} \tag{7}$$

where $P_{\mathrm{PV}}^{\mathrm{MPPT}}$ is the output power with MPPT mode; k_{PV}^{dc} and k_{PV}^{ac} are the PV' s droop coefficients in dc side and ac side, respectively; and $f_{\max}$ and $V_{dc}^{\max}$ are the allowable maximum frequency and the allowable maximum dc voltage, respectively.

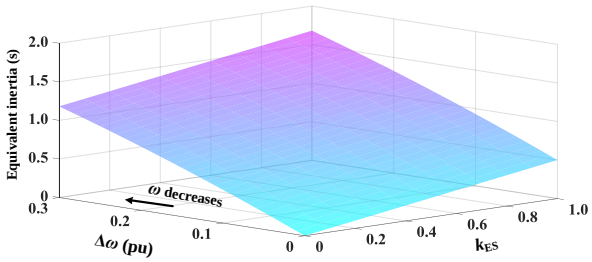

Fig. 5. $H_{\mathrm{W\_E}}^{\mathrm{STIS}}$ variation with the changes of k_{ES} and $\Delta\omega$.

MTG implemented in the hybrid network will serve as auxiliary power source. More specifically, it can be activated and output active power according to the variation of frequency and dc voltage caused by net power deficit. Thus, the MTG is controlled in the opposite operational quadrant of the PV panel.

C. Inertial Response of WTG with HESs.

WTG is a kind of DG with rotational component, which can release kinetic energy [31], [32]. More specifically, WTG works in MPPT mode to make full use of wind power, and may slow down the mechanical rotor speed, denoted as ω_r, to release certain amount of kinetic energy to provide STIS when there is net power deficit. The equivalent inertia of WTG serving for STIS can be expressed as

$$H_{\mathrm{WTG}}^{\mathrm{STIS}}=\frac{\frac{1}{2}J_W(\omega_{\mathrm{MPPT}}^2-\omega_r^2)}{S_{\mathrm{WTG}}}=\frac{\Delta P_{\mathrm{WTG}}^{\mathrm{STIS}}}{S_{\mathrm{WTG}}}\Delta t \tag{8}$$

where

$$\Delta P_{\mathrm{WTG}}^{\mathrm{STIS}}=-\frac{\mathrm{d}W_{\mathrm{WTG}}}{\mathrm{d}t}=-J_W\omega_r\frac{\mathrm{d}\omega_r}{\mathrm{d}t} \tag{9}$$

where $H_{\mathrm{WTG}}^{\mathrm{STIS}}$ is the equivalent inertia constant of WTG, J_W is the moment of inertia of WTG, ω_{MPPT} is the stable rotor speed in MPPT mode, $\Delta P_{\mathrm{WTG}}^{\mathrm{STIS}}$ is the increasing power of WTG for STIS, and Δt is the duration time of STIS, respectively.

HES unit can be used to assist the WTG in STIS. Assuming the auxiliary power of HES unit is proportional to $\Delta P_{\mathrm{WTG}}^{\mathrm{STIS}}$, which means $\Delta P_{\mathrm{ES}}^{\mathrm{STIS}}=k_{\mathrm{ES}}\times\Delta P_{\mathrm{WTG}}^{\mathrm{STIS}}$, the inertia response power of WTG will be shared in part by ES by adjusting the value of coefficient k_{ES}. Substituting this relationship and $\Delta\omega=\omega_{\mathrm{MPPT}}-\omega_r$ into (8), and consider the contribution of HES unit, then the equivalent inertial constant for the WTG-HES combined system, denoted as $H_{\mathrm{W\_E}}^{\mathrm{STIS}}$, is defined as

$$\begin{aligned}H_{\mathrm{W\_E}}^{\mathrm{STIS}}&=\frac{J_W\omega_{\mathrm{MPPT}}\Delta\omega-\frac{1}{2}J_W\Delta\omega^2+k_{\mathrm{ES}}\Delta P_{\mathrm{WTG}}^{\mathrm{STIS}}\Delta t}{S_{\mathrm{WTG}}}\\&=\frac{2(k_{\mathrm{ES}}\Delta P_{\mathrm{WTG}}^{\mathrm{STIS}}\Delta t+J_W\omega_{\mathrm{MPPT}}\Delta\omega)-J_W\Delta\omega^2}{2S_{\mathrm{WTG}}}\end{aligned} \tag{10}$$

It can be seen from (10) that, with the fixed support power $\Delta P_{\mathrm{WTG}}^{\mathrm{STIS}}$ (corresponding to fixed $H_{\mathrm{W\_E}}^{\mathrm{STIS}}$), the participation of HES will reduce the slowdown of rotor speed during STIS. Fig. 5 gives the illustration of how the HESs and rotor speed slowdown can contribute to $H_{\mathrm{W\_E}}^{\mathrm{STIS}}$. It should be noted that in practice, the value of $\Delta\omega$ is usually less than 0.3 pu to avoid possible rotor halt. As is shown, the contribution of HES unit will be important when the WTG operates at a low speed, and k_{ES} should be determined carefully according to the analysis above.

More specifically, the value of k_{ES} can be set in the range

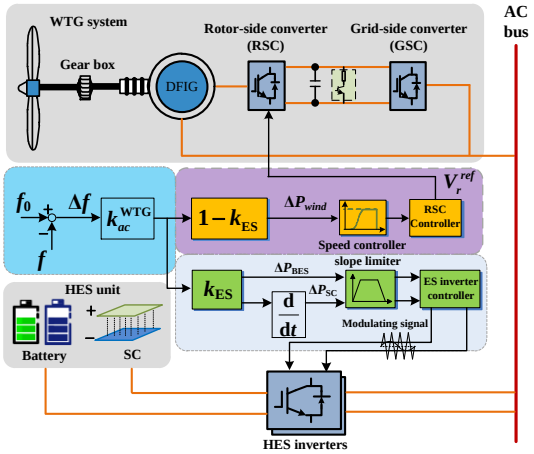

Fig. 6. Schematic design of the inertial response controller of WTG-HES combined system.

between 0 and 1. On one hand, the larger value of k_{ES} means the HES unit will take more power burden of inertial support, and reduce the additional output power of WTG, leading to less speed slowing down. However, the HES unit combined with WTG is generally for reducing high-frequency wind power fluctuation, which features small capacity, and it is possible to run out of HES energy with large k_{ES}. On the other hand, the smaller value of k_{ES} means WTG will shoulder much power burden for the additional inertial support, which may cause rotor halt or second frequency/voltage drop.

As shown in (4), the fast power support is realized by responding to the differential terms of frequency and dc voltage. Besides, the system will also activate the primary frequency regulation (for ac system) and voltage droop control (for dc system) to ensure the system stability. Therefore, the inertial response power for WTG-HES system is defined as,

$$\Delta P_{\mathrm{W\_ES}}^{\mathrm{STIS}}=\begin{cases}-k_{ac}^{\mathrm{WTG}}\dfrac{\mathrm{d}f}{\mathrm{d}t}+k_{ac}^{\mathrm{WTG}}(f_0-f), & \text{for ac nanogrid}\\ -k_{dc}^{\mathrm{WTG}}V_{dc}\dfrac{\mathrm{d}V_{dc}}{\mathrm{d}t}+k_{dc}^{\mathrm{WTG}}(V_{ref}-V_{dc}), & \text{for dc nanogrid}\end{cases} \tag{11}$$

where k_{ac}^{WTG} and k_{dc}^{WTG} are the WTG's droop coefficients of ac side and dc side, respectively.

This article has been accepted for publication in a future issue of this journal, but has not been fully edited. Content may change prior to final publication. Citation information: DOI 10.1109/TSG.2019.2942736, IEEE Transactions on Smart Grid

It should be noted that at the start moment of power variation, the value of differential terms in inertia response is far larger than the linear ones. Hence, it is proper for SC, which features large power density, to be responsible for the transient large power vacancy (i.e., the high-frequency component of power demand). Taking the scenario in ac nanogrid as an example, the power assignment in HES can be designed as

$$\Delta P_{\mathrm{ES}}^{\mathrm{STIS}} = \underbrace{k_{\mathrm{ES}} k_{ac}^{\mathrm{WTG}} (f_0 - f)}_{\text{Battery response}} + \underbrace{(-k_{\mathrm{ES}} k_{ac}^{\mathrm{WTG}} \frac{\mathrm{d}f}{\mathrm{d}t})}_{\text{SC response}} \tag{12}$$

Fig. 6 gives the schematic design of the proposed coordinated controller, which is an example in ac nanogrid. When there exists a frequency variation, the controller will determine k_{ES} according to characteristics shown in Fig. 5, and the reference output power for frequency support of WTG and the HES unit can be obtained by calculating the value of Δf and its differential term, where the control is realized by adjusting the reference voltage of RSC, and changing the modulating signal of HES's inverter, which ensures the inertial support can be achieved. It is worth noting that, there are two control signals, i.e. ΔP_{BES} and ΔP_{SC}, sent to the HES unit in Fig. 6. And the BES and SC are connected to two individual converters to ensure they can respond to different control component.

D. Local Inertial Support with HESs

The distributed HESs should be responsible for the local power disturbance, which generally adopt the droop control method to compensate for the variation of voltage and frequency. Unlike the fixed-coefficient droop principle, an improved droop method is proposed, in which the droop coefficient is adaptively varied according to the differential term in (4), and can be expressed as

$$\Delta P_{\mathrm{LS}}^{\mathrm{HES}} = \begin{cases} k_{ac}^{\mathrm{HES}} \exp(2H_{vir}^{\mathrm{ES}} \left|\frac{\mathrm{d}f}{\mathrm{d}t}\right|) \Delta f, & \text{for ac nanogrid} \\ k_{dc}^{\mathrm{HES}} \exp(C_{vir}^{\mathrm{ES}} V_{dc} \left|\frac{\mathrm{d}V_{dc}}{\mathrm{d}t}\right|) \Delta V_{dc}, & \text{for dc nanogrid} \end{cases} \tag{13}$$

where k_{ac}^{HES} and k_{dc}^{HES} are the HES's droop coefficients of ac and dc side, respectively; H_{vir}^{ES} and C_{vir}^{ES} are the virtual inertial constant of HES and the virtual capacitance of HES, respectively.

In the improved droop method, the equivalent droop coefficient can vary during transient state, and provide more power support. Taking the local inertial support with HESs in ac nanogrid as the example, when there appears a frequency drop, the value of exponential term will increase sharply due to the significant change of df/dt, which leads to a larger value of the equivalent droop coefficient. Hence, $\Delta P_{\mathrm{LS}}^{\mathrm{HES}}$ will be larger than that of fixed droop method, which means the proposed method provides more power during transient state and the inertial response can be improved. When the system converges to steady state, the frequency derivative will decrease to zero, and the droop coefficient returns to the preset value. The visualized comparison can be seen in Fig. 7. Therefore, the proposed method can improve the transient inertial response without changing the system steady state.

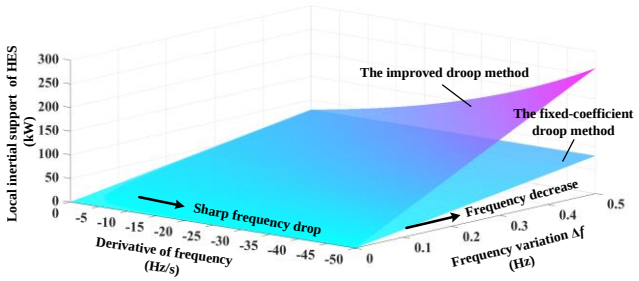

Fig. 7. Comparison between two droop methods for local inertial support with HESs in ac nanogrid (settings: k_{ac}^{HES}=160 kW/Hz, H_{vir}^{ES}=0.012 s).

Notice that the output power of battery energy storage (BES) has the limited ramp rate, whereas the SC can be considered with infinite power density. Thus, for the protection of BES and better utilization of SC's advantage, the power demand $\Delta P_{\mathrm{LS}}^{\mathrm{HES}}$ is processed using the low-pass filter and assigned to different ES equipment. After this operation, SC is only responsible for the high-frequency component which can be described as,

$$\Delta P_{\mathrm{LS}}^{\mathrm{SC}} = \Delta P_{\mathrm{LS}}^{\mathrm{HES}} \frac{sT}{1+sT} \tag{14}$$

where T is the time constant of the filter.

When the type of BES device is determined (e.g., Li-ion battery), the larger installation number of BES will correspond to smaller T value.

E. Cross-grid Inertial Support with Distributed HESs and IC.

The cross-grid inertia support can be realized by employing the power support capacity of distributed HESs. Considering that ac frequency usually varies in a small range (less than ±0.005p.u.), the linearizing relationship of ac and dc grids can be derived from (5) and expressed as

$$\Delta V_{dc} = \frac{2H_{\mathrm{VSG}} S_{\mathrm{IC}}}{V_{ref} C_{\mathrm{VC}} f_0} \Delta f = k_c \Delta f \tag{15}$$

where k_c is the coupling coefficient of voltage and frequency.

When the power deficiency occurs in dc nanogrid, the voltage variation will be detected and leads to a corresponding change of Δf according to (15), which is re-denoted as Δf_{vir} to tell apart from the real frequency change. Then, the droop equation of HES in ac grid can be adjusted to consider the virtual frequency change derived from ΔV_{dc} and expressed by

$$\Delta P_{ac}^{\mathrm{HES}} = k_{ac}^{\mathrm{HES}} \exp(2H_{vir}^{\mathrm{ES}} \left|\frac{\mathrm{d}f}{\mathrm{d}t}\right|)(\Delta f + \Delta f_{vir}) \tag{16}$$

To involve the dynamic feature of inertia response in dc grid, substituting Δf_{vir} into the left part of (4) and combining with (16) can lead to the power reference of HES in ac grid as the following,

$$\Delta P_{ac}^{\mathrm{HES}} = k_{ac}^{\mathrm{HES}} \exp(2H_{vir}^{\mathrm{ES}} \left|\frac{\mathrm{d}f}{\mathrm{d}t}\right|)(\Delta f + \Delta f_{vir}) - \frac{k_c^2 C_{\mathrm{VC}}}{S_{\mathrm{IC}}} f_0 \frac{d\Delta f_{vir}}{dt} \tag{17}$$

Similarly, when the power deficiency occurs in ac nanogrid, the frequency variation will be detected and leads to a corresponding change of ΔV_{dc}, which is re-denoted as ΔV_{vir} to tell apart from the real voltage change. Then, the droop equation of HES in dc grid can be adjusted to consider the virtual voltage change derived from Δf and expressed by,

This article has been accepted for publication in a future issue of this journal, but has not been fully edited. Content may change prior to final publication. Citation information: DOI 10.1109/TSG.2019.2942736, IEEE Transactions on Smart Grid

$$\Delta P_{dc}^{\mathrm{HES}} = k_{dc}^{\mathrm{HES}} \exp(C_{vir}^{\mathrm{ES}} V_{dc} \left|\frac{\mathrm{d}V_{dc}}{\mathrm{d}t}\right|)(\Delta V_{dc} + \Delta V_{vir}) \quad (18)$$

To emulate the dynamic feature of inertia response in ac grid, substituting ΔV_{vir} into the right part of (4) and combining with (18) can lead to the power reference of HES in dc grid as the following,

$$\Delta P_{dc}^{\mathrm{HES}} = k_{dc}^{\mathrm{HES}} \exp(C_{vir}^{\mathrm{ES}} V_{dc} \left|\frac{\mathrm{d}V_{dc}}{\mathrm{d}t}\right|)(\Delta V_{dc} + \Delta V_{vir}) - \frac{2H_{\mathrm{VSG}}}{k_c f_0}\frac{d\Delta V_{vir}}{dt} \quad (19)$$

The IC is used to transfer power between ac and dc nanogrids, and the difference between the cross-grid power of distributed HESs is set as the power reference of IC, which is described as,

$$\begin{aligned}\Delta P_{\mathrm{IC}} = &[\Delta P_{ac}^{\mathrm{HES}} - k_{ac}^{\mathrm{HES}} \exp(2H_{vir}^{\mathrm{ES}} \left|\frac{\mathrm{d}f}{\mathrm{d}t}\right|)\Delta f] \\ &-[\Delta P_{dc}^{\mathrm{HES}} - k_{dc}^{\mathrm{HES}} \exp(C_{vir}^{\mathrm{ES}} V_{dc} \left|\frac{\mathrm{d}V_{dc}}{\mathrm{d}t}\right|)\Delta V_{dc}]\end{aligned} \quad (20)$$

It should be noted that, if there are more than one IC, ΔP_{IC} will be proportionally assigned to ICs according to each IC's rated power. Based on the coordinated design above, the cross-grid inertial control can be realized through the coordination of the IC and the distributed HESs in hybrid system, as shown in Fig. 8. Since the exponential term is used in local and cross-grid inertial support of HESs, the limiter blocks are added in the control loops to constrain the reference power magnitude of HESs. It is worth noting that, whatever control methods are adopted, the limiter block is necessary to restrict the control signal that exceeds the power limits of HES unit for protection, and its value is usually determined by the maximum power of the HES unit. In this paper, the limiter setting is accordance with the maximum power that HES can absorb and output, which is chosen as 100 kW.

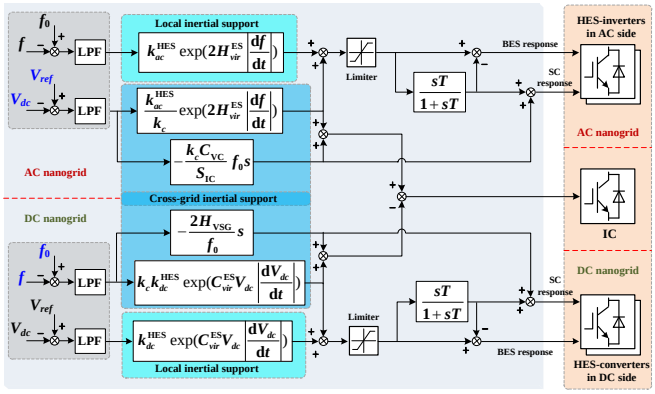

Fig. 8. Coordinated control of local and cross-grid inertial support of HES.

IV. Case Studies

To validate the proposed strategy, a simulation model of hybrid microgrid is established based on Fig. 1. HES unit is composed of Li-on battery and SC, where the ramp rate of BES is set as 95 kW/s, and SC is considered with infinite output power speed [38]. The time constant for filter used for the local inertial support of HES is 0.5 s, and k_{ES} for WTG system is set as 0.4. Other parameters of the system are given in Table I.

TABLE I
Parameters of the Studied Hybrid Microgrid

Sub-systems	*Items*	*Values*
AC nanogrid	Nominal frequency/Hz	50
	Droop coefficient of WTG/(kW/Hz) $k_{\mathrm{ac}}^{\mathrm{WTG}}$	130
	Droop coefficient of HES/(kW/Hz) $k_{\mathrm{ac}}^{\mathrm{HES}}$	160
	Virtual inertial constant of HES/s H_{vir}^{ES}	0.012
	Correlation inertial constant/s H_{VSG}	0.065
	Rated capacity/kVA	500
DC nanogrid	Nominal voltage/V	660
	Rated capacity/kW	500
	Droop coefficient of WTG/(kW/V) $k_{\mathrm{dc}}^{\mathrm{WTG}}$	3
	Droop coefficient of HES/(kW/V) $k_{\mathrm{dc}}^{\mathrm{HES}}$	6.8
	Virtual capacitance of HES/mF C_{vir}^{ES}	1.5
	Correlation capacitance/mF C_{VC}	7.5
IC	Rated capacity/kVA	500

Two different scenarios are compared: the only droop strategy and the proposed strategy. The only droop strategy features that the conventional droop control shall be activated during power disturbance, including the local power compensation and cross-grid power support [4], [11], of which the droop coefficients are as same as that of the proposed strategy. It is worth noting that, the frequency and voltage responses without cross-grid support (i.e. only local droop response without inertial compensation activated) are also shown for comparison.

A. Case 1: Step Power Variation in AC Side

This case is to show the performance of the proposed strategy on inertial improvement for ac nanogrid, and the results are shown in Figs. 9 and 10, and Table II, where change rate is obtained when the variables change from the stable value to the extremum value. When the load power increment of 50 kW is activated at 2 s at the ac side, a frequency drop is shown in Fig. 9(a), which indicates that the frequency variation is smoothed with the proposed strategy and also less overshoot is caused when the power demand is reduced at 7 s. Compared with the only-droop control, the dc voltage variation is a little larger with the inertial support, shown in Fig. 9(b), since the dc side provides more active power to support ac side's inertia.

Notice that the unified inertia variation keeps smaller with our strategy during the whole power changes, shown in Fig. 9(c), which means the strategy features better dynamic performance, and thus the system robustness is increased. More specifically, when the load power increment of 50 kW occurs at 2 s in the ac side, and the unified inertia H_u drops to 3.97 s immediately with the only-droop control. In comparison, H_u smoothly drops to 3.992 s at the same time point with the proposed strategy as shown in Fig. 9(c). From the analysis in Section II. A we can see, during the normal operational condition, the allowable maximum variation range of H_u is 0.32 s (i.e., from 3.845 s to 4.165 s), so the proposed strategy reduces the decrease of holistic inertia from 9.3% to 2.5% (using 0.32 s as the base) during transient state. In addition, Table II gives the change rate of f, V_{dc}, and H_u, which is defined by the duration time when these variables change from steady value to the extremum in transient state. As is shown, during 2-7s, the ab-

This article has been accepted for publication in a future issue of this journal, but has not been fully edited. Content may change prior to final publication. Citation information: DOI 10.1109/TSG.2019.2942736, IEEE Transactions on Smart Grid

solute value of H_u change rate can be as large as 0.03 with the only-droop control, and reduce to 0.01 with the proposed strategy, which indicates a clear improvement for system inertia.

Fig. 10 shows the power assignment of HES equipment and the IC power variation. It can be seen that, the power demand is properly distributed to BES and SC, which is reflected by the ramp rates within the limit (i.e., 95kW/s) at both ac and dc sides. Besides, the output power of HES in ac side (approaching 22 kW) is larger than that of dc side, since the power variation occurs in ac nanogrid, and will not bring much burden to the HES unit of dc side. It is worth noting that, with the introduction of derivative terms to emulate inertial response, the power response of IC will be faster than that of only-droop control, as shown in Fig. 10(c), which contributes to the smoother change of frequency.

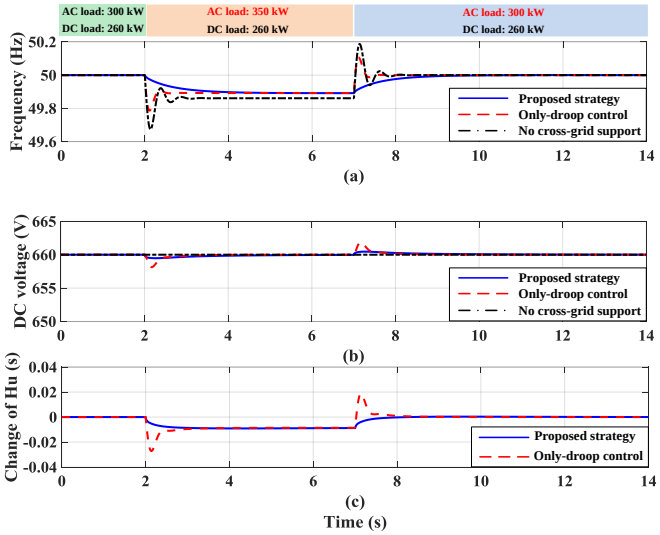

Fig. 9. Variations of indexes in case 1. (a) Frequency variation. (b) DC voltage variation. (c) Variation of the unified inertia.

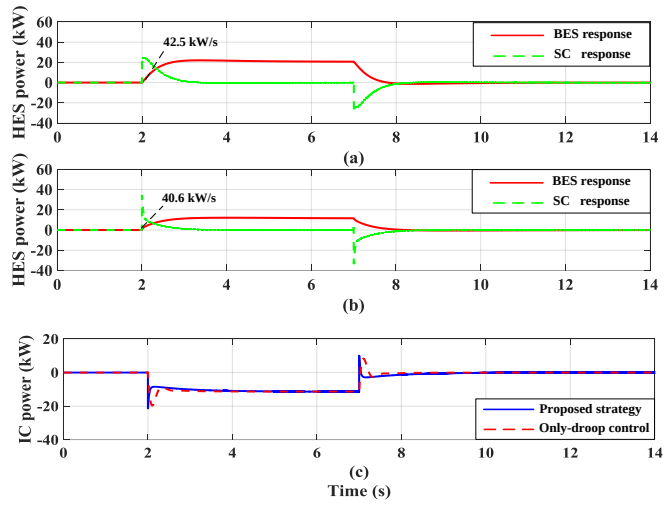

Fig. 10. Active power in case 1. (a) HES power in ac nanogrid. (b) HES power in dc nanogrid. (c) IC power.

TABLE II
CHANGE RATE DURING TRANSIENT STATE (CASE 1)

Variable	Scenarios	0-2 s	2-7 s	7-14 s
Frequency change rate (Hz/s)	Proposed strategy	0	-0.08	0.09
	Only-droop control	0	-2.21	2.63
DC voltage change rate (V/s)	Proposed strategy	0	-2.5	3.0
	Only-droop control	0	-10.1	12.5
Unified inertia change rate (pu)	Proposed strategy	0	-0.01	0.01
	Only-droop control	0	-0.30	0.30

B. *Case 2: Step Power Variation in DC Side.*

A net power increment of 100 kW is activated at 2 s in dc side, which causes an immediate voltage drop to 648 V with the only-droop method as shown in Fig. 11(a). In comparison, the voltage decreases slowly to the lowest value after 4 s, which releases the pressure of equipment and brings more response time for other DGs. As shown in Fig. 11(b), the mutual power support has little influence on frequency in ac side.

The clear improvement can be seen in Table III, in which the absolute value of H_u change rate reduces from 0.42 to 0.02. Besides, as shown in Fig. 11(11), the maximum decrease of H_u with the only-droop control is 0.081 s at 2.2 s with H_u dropping to 3.919 s. In comparison, H_u keeps the higher value of 3.962 s at the same time point with the proposed method. By normalizing the maximum variation at 2.2 s using the allowable variation (i.e., 0.32 s) in normal operation, H_u decrease reduces from 25.31% to 11.88%, which indicates the effectiveness of the proposed inertial compensation method for dc nanogrid.

The output power of HESs are illustrated in Fig. 12, where much power burden is allocated to the HES unit in dc side, and the largest ramp rate is 76.3 kW/s within the limit. As shown in Fig. 12(c), the IC power increases to the higher value with the only-droop control, since the voltage drops to lower level and it needs more power to keep balance. In comparison, the power increment of IC with the proposed strategy is larger at the initial moment, and then becomes mild between 2.2 s and 8 s, indicating that the IC power burden is released with better dc voltage performance.

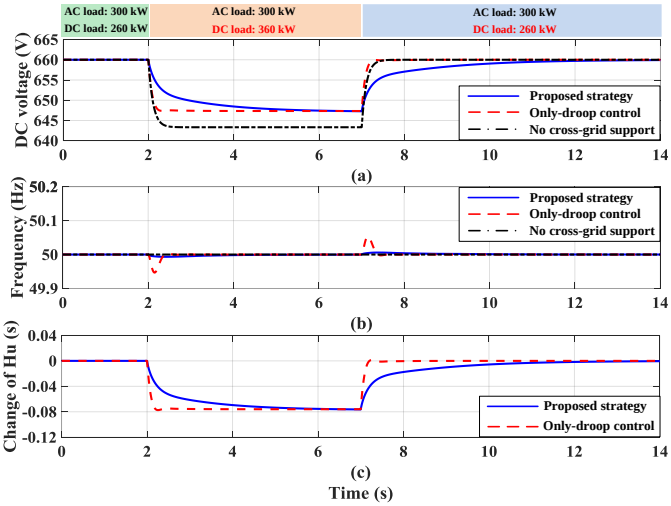

Fig. 11. Variation of indexes in case 2. (a) DC voltage variation. (b) Frequency variation. (c) Variation of the unified inertia.

This article has been accepted for publication in a future issue of this journal, but has not been fully edited. Content may change prior to final publication. Citation information: DOI 10.1109/TSG.2019.2942736, IEEE Transactions on Smart Grid

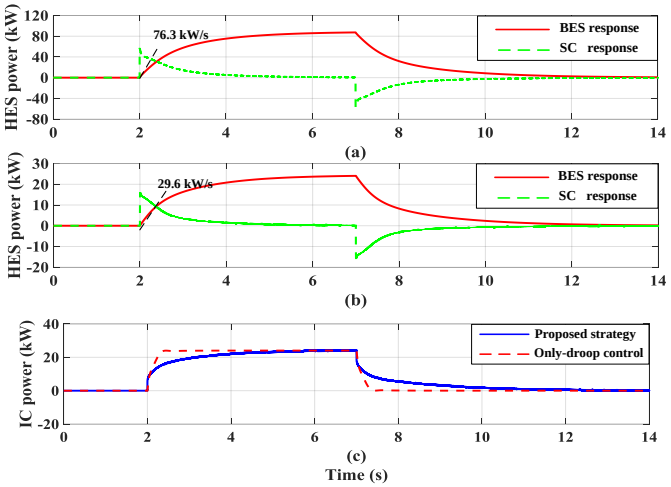

Fig. 12. Active power in case 2. (a) HES power in dc nanogrid. (b) HES power in ac nanogrid. (c) IC power.

TABLE III
CHANGE RATE DURING TRANSIENT STATE (CASE 2)

Variable	Scenarios	0-2 s	2-7 s	7-14 s
Frequency change rate (Hz/s)	Proposed strategy	0	-0.03	0.04
	Only-droop control	0	-0.27	0.26
DC voltage change rate (V/s)	Proposed strategy	0	-3.7	3.5
	Only-droop control	0	-68.4	68.2
Unified inertia change rate (pu)	Proposed strategy	0	-0.02	0.02
	Only-droop control	0	-0.42	0.42

C. Case 3: Consecutive Power Variation in Both Sides.

The net power increment of 50 kW in ac nanogrid is activated at 2 s, leading to the frequency drop, which is the same as that in case 1. At 6 s, the net power increase of 100 kW at dc side occurs, and the IC transferring power is changed from -10.73 kW to 13.32 kW according to (20), shown in Fig. 14(c). It is worth noting that, there is no evident variation of the ac frequency with the proposed strategy. In comparison, the frequency with the only-droop control drops to 49.83 Hz and then recovers to stability [see Fig. 13(a)]. It can be concluded that, when there are power variations in both sides, the proposed strategy can adaptively realize the reasonable power assignment for IC. More specifically, the variation, corresponding to deterioration of voltage or frequency, will not be transported to the other side during the mutual power support, so the mutual inertial support will not bring negative effect on the power provider side, which is reflected by the smooth frequency curve with the proposed strategy at 6 s.

At 9 s and 12 s, the net power decreases are activated in ac and dc nanogrids, respectively. It can be seen from Fig. 13, the overshoots of f and V_{dc} are avoided, which shows the dynamic performance improvement with the proposed strategy. Besides, Fig. 14(c) indicates that the good inertial support should be attributed to the fast response of IC power (i.e. sharp transient power variation), which takes advantage of the merits of the converter and SC.

As can be seen from Table IV, no matter the net power deficit (e.g., 3s and 6s) or surplus (e.g., 9s and 12s) occurs, the system inertia, reflected by H_u, varies with relatively small change rate with the proposed strategy. The maximum power deficit occurs at 6s when both the ac and dc nanogrid experience total 150 kW load power increment, the severe variation of Hu is reduced from 24.69% to 12.51% reflected in Fig. 13(c), which shows the performance of cross-grid inertial support.

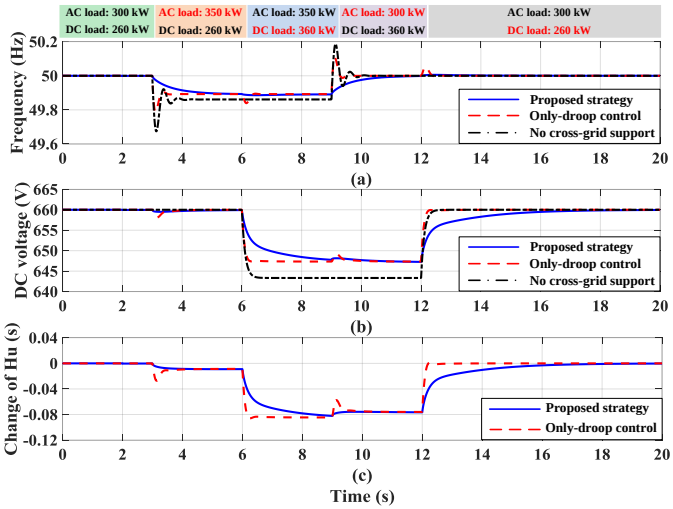

Fig. 13. Variation of indexes in case 3. (a) Frequency variation. (b) DC voltage variation. (c) Variation of the unified inertia.

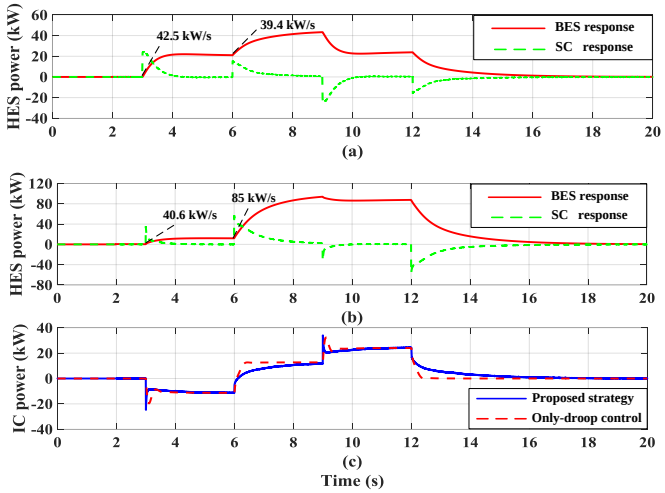

Fig. 14. Active power in case 3. (a) HES power in ac nanogrid. (b) HES power in dc nanogrid. (c) IC power.

TABLE IV
CHANGE RATE DURING TRANSIENT STATE (CASE 3)

Variable	Scenarios	3-6 s	6-9 s	9-12s	12-20s
Frequency change rate (Hz/s)	Proposed strategy	-0.08	-0.05	0.04	0.01
	Only-droop control	-2.21	-0.37	1.15	0.45
DC voltage change rate (V/s)	Proposed strategy	-2.5	-4.32	2.38	2.47
	Only-droop control	-10.1	-68.42	7.52	63.15
Unified inertia change rate (pu)	Proposed strategy	-0.01	-0.03	0.05	0.02
	Only-droop control	-0.30	-0.27	0.18	0.41

V. CONCLUSION

In this paper, a comprehensive inertial improvement strategy, which fully takes advantage of the features of various DGs, is proposed for hybrid ac/dc microgrid. The unified inertial is introduced to indicate the global inertial level of the hybrid system, and the coupling relationship of ac and dc grids is expressed for cross-grid inertial support. The design of the strategy is based on the power capacity of different DGs, real-

izes the reasonable power assignment among DGs and enhance the global inertial stability. Further, the local and cross-grid power sharing are designed to exploit the power capacity of distributed HESs, which can realize the net power balance with good dynamic response and improve the system's robustness. Moreover, the ramp rate difference between BES and SC is considered to facilitate better utilization, and contributes to the operational lifespan of different ES units. The effectiveness of the strategy is validated by the simulation cases with several scenarios.

REFERENCES

[1] J. M. Guerrero, P. C. Loh, T.-L. Lee, and M. Chandorkar, "Advanced control architectures for intelligent microgrids—Part II: Power quality, energy storage, and AC/DC microgrids," *IEEE Trans. Ind. Electron.*, vol. 60, no. 4, pp. 1263–1270, Apr. 2013.

[2] F. Nejabatkhah and Y. W. Li, "Overview of power management strategies of hybrid AC/DC microgrid," *IEEE Trans. Power Electron.*, vol. 30, no. 12, pp. 7072–7089, Dec. 2015.

[3] M. Khooban, "Secondary load frequency control of time-delay standalone microgrids with electric vehicles," *IEEE Trans. Ind. Electron.*, vol. 65, no. 9, pp. 7416-7422, Sept. 2018.

[4] N. Eghtedarpour and E. Farjah, "Power control and management in a hybrid AC/DC microgrid," *IEEE Trans. Smart Grid*, vol. 5, no. 3, pp. 1494-1505, May 2014.

[5] H. Bevrani, T. Ise, and Y. Miura, "Virtual synchronous generators: A survey and new perspectives," *Int. J. Elect. Power Energy Syst.*, vol. 54, pp. 244-254, Jan. 2014.

[6] M. Jafari, Z. Malekjamshidi, J. Zhu, and M. Khooban, "Novel predictive fuzzy logic-based energy management system for grid-connected and off-grid operation of residential smart micro-grids," *IEEE J. Emerg. Sel. Topics Power Electron.*, doi:10.1109/JESTPE.2018.2882509.

[7] S. M. Malik, X. Ai, Y. Sun, Z. Chen, and S. Zhou, "Voltage and frequency control strategies of hybrid AC/DC microgrid: A review," *IET Gener., Transmiss. Distrib.*, vol. 11, no. 2, pp. 303–313, 2017.

[8] J. M. Guerrero, M. Chandorkar, T.-L. Lee, and P. C. Loh, "Advanced control architectures for intelligent microgrids – Part I: Decentralized and hierarchical control," *IEEE Trans. Ind. Electron.*, vol. 60, no. 4, pp. 1254–1262, Apr. 2013.

[9] D. E. Olivares, C. A. Canizares, and M. Kazerani, "A centralized energy management system for isolated microgrids," *IEEE Trans. Smart Grid*, vol. 5, no. 4, pp. 1864–1875, Jul. 2014.

[10] P. Wang, C. Jin, D. Zhu, Y. Tang, P. C. Loh, and F. H. Choo, "Distributed control for autonomous operation of a three-port AC/DC/DS hybrid microgrid," *IEEE Trans. Ind. Electron.*, vol. 62, no. 2, pp. 1279–1290, Feb. 2015.

[11] X. Liu, P. Wang, and P. C. Loh, "A Hybrid AC/DC Microgrid and Its Coordination Control," *IEEE Trans. Smart Grid*, vol. 2, no. 2, pp. 278-286, Jun. 2011.

[12] J. Wang, C. Jin, and P. Wang, "A uniform control strategy for the interlinking converter in hierarchical controlled hybrid AC/DC microgrids," *IEEE Trans. on Ind. Electron*, vol. 65, no. 8, pp. 6188-6197, Aug. 2018.

[13] Q. Xu, J. Xiao, P. Wang, and C. Wen, "A decentralized control strategy for economic operation of autonomous AC, DC, and hybrid AC/DC microgrids," *IEEE Trans. Energy Convers.*, vol. 32, no. 4, pp. 1345-1355, Dec. 2017.

[14] X. Lu, J. M. Guerrero, K. Sun, J. C. Vasquez, R. Teodorescu, and L. Huang, "Hierarchical Control of Parallel AC-DC Converter Interfaces for Hybrid Microgrids," *IEEE Trans. Smart Grid*, vol. 5, no. 2, pp. 683-692, Mar. 2014.

[15] P. Kundur, Power systems stability and control. New York, NY, USA: McGraw-Hill, 1993.

[16] Q.-C. Zhong and G. Weiss, "Synchronverters: Inverters that mimic synchronous generators," *IEEE Trans. Ind. Electron.*, vol. 58, no. 4, pp. 1259–1267, Apr. 2011.

[17] D. Li, Q. Zhu, S. Lin, and X.Y. Bian, "A self-adaptive inertia and damping combination control of VSG to support frequency stability," *IEEE Trans. Energy Convers.*, vol. 32, no, 1, pp. 397-398, Nov. 2016.

[18] Y. Karimi, H. Oraee, and J. M. Guerrero, "Decentralized method for load sharing and power management in a hybrid single/three-phase-islanded microgrid consisting of hybrid source PV/battery units," *IEEE Trans. Power Electron.*, vol. 32, no. 8, pp. 6135–6144, Aug. 2017.

[19] A. A. El-Fergany and M. A. El-Hameed, "Efficient frequency controllers for autonomous two-area hybrid microgrid system using social-spider optimiser," *IET Gener., Transmiss. Distrib.*, vol. 11, no. 3, pp. 637-648, 2017.

[20] T. Kerdphol, F. S. Rahman, Y. Mitani, M. Watanabe and S. Küfeoğlu, "Robust virtual inertia control of an islanded microgrid considering high penetration of renewable energy," *IEEE Access*, vol. 6, pp. 625-636, 2018.

[21] S. Augustine, M. K. Mishra, and N. Lakshminarasamma, "Adaptive droop control strategy for load sharing and circulating current minimization in low-voltage standalone DC microgrid," *IEEE Trans. Sustain. Energy*, vol. 6, no. 1, pp. 132–141, Jan. 2015.

[22] X. Lu, J. M. Guerrero, K. Sun, and J. C. Vasquez, "An improved droop control method for DC microgrids based on low bandwidth communication with DC bus voltage restoration and enhanced current sharing accuracy," *IEEE Trans. Power Electron.*, vol. 29, no. 4, pp. 1800-1812, April 2014.

[23] J. Xiao, P. Wang, and L. Setyawan, "Multilevel energy management system for hybridization of energy storages in DC microgrids," *IEEE Trans. Smart Grid*, vol.7, no.2, pp.847-856, Mar. 2016.

[24] T. Morstyn, B. Hredzak, G. D. Demetriades, and V. G. Agelidis, "Unified distributed control for DC microgrid operating modes," *IEEE Trans. Power Syst.*, vol. 31, no. 1, pp. 802–812, Jan. 2016.

[25] S. Samanta, J. P. Mishra, and B. K. Roy, "Virtual DC machine: an inertia emulation and control technique for a bidirectional DC–DC converter in a DC microgrid," *IET Electric Power Applications*, vol. 12, no. 6, pp. 874-884, 2018.

[26] A. B. Attya, J. L. Dom ínguez-Garc á, F. D. Bianchi, and O. Anaya-Lara, "Enhancing frequency stability by integrating non-conventional power sources through multi-terminal HVDC grid," *Int. J. Elect. Power Energy Syst.*, vol. 95, pp. 128-136, Sept. 2018.

[27] H. Zhao, M. Hong, W. Lin, and K. A. Loparo, "Voltage and frequency regulation of microgrid with battery energy storage systems," *IEEE Trans. Smart Grid*, vol. 10, no. 1, pp. 414–424, Jan. 2019.

[28] N. Korada and M. K. Mishra, "Grid adaptive power management strategy for an integrated microgrid with hybrid energy storage," *IEEE Trans. Ind. Electron.*, vol. 64, no. 4, pp. 2884–2892, Apr. 2017.

[29] Q. Xu, X. Hu, P. Wang, J. Xiao, P. Tu, C. Wen, and M. Y. Lee, "A decentralized dynamic power sharing strategy for hybrid energy storage system in autonomous DC microgrid," *IEEE Trans. Ind. Electron.*, vol. 64, no. 7, pp. 5930-5941, July 2017.

[30] J. Li, S. Wang, L. Ye, and J. Fang, "A coordinated dispatch method with pumped-storage and battery-storage for compensating the variation of wind power," *Prot. Control Mod. Power Syst*, vol. 3, no. 3, pp. 21-34, Dec. 2018.

[31] Y. Li, L. He, F. Liu, Y. Tan, Y. Cao, L. Luo, and M. Shahidehpour, "A dynamic coordinated control strategy of WTG-ES combined system for short-term frequency support", *Renewable Energy*, vol. 119, pp. 1–11, 2018.

[32] A. B. Attya, S. Ademi, M. Jovanović, and O. Anaya-Lara, "Frequency support using doubly fed induction and reluctance wind turbine generators," *Int. J. Elect. Power Energy Syst.*, vol. 101, pp. 403-414, Apr. 2018.

[33] A. Junyent-Ferr é, Y. Pipelzadeh, and T. C. Green, "Blending HVDC-link energy storage and offshore wind turbine inertia for fast frequency response," *IEEE Trans. Sustain. Energy*, vol. 6, no. 3, pp. 1059-1066, 2015.

[34] Y. Li, L. He, F. Liu, C. Li, Y. Cao, and M. Shahidehpour, "Flexible voltage control strategy considering distributed energy storages for DC distribution network," *IEEE Transactions on Smart Grid*, vol.10, no.1, pp.163-172, Jan. 2019.

[35] L. He, Y. Li, Z. Shuai, J. M. Guerrero, Y. Cao, M. Wen, W. Wang, and J. Shi, "A flexible power control strategy for hybrid AC/DC zones of shipboard power system with distributed energy storages," *IEEE Transactions on Industrial Informatics*, vol. 14, no. 12, pp. 5496-5508, Dec. 2018.

[36] M. Dehghani, M. H. Khooban, T. Niknam, and S. M. Rafiei, "Time-varying sliding mode control strategy for multibus low-voltage microgrids with parallel connected renewable power sources in islanding mode," *J. Energy Eng.*, vol. 142, no. 4, Feb. 2016.

[37] Q. Liu, Y. Li, L. Luo, Y. Peng, and Y. Cao, "Power Quality Management of PV Power Plant with Transformer Integrated Filtering Method," *IEEE Transactions on Power Delivery*, vol. 34, no. 3, pp. 941-949, June 2019.

[38] D. L. Zhang, J. L. Li, and D. Hui, "Coordinated control for voltage regulation of distribution network voltage regulation by distributed en-

ergy storage systems," *Prot. Control Mod. Power Syst.*, vol. 3, no. 1, pp. 35-42, Dec.2018.

Li He (S'16) was born in Hunan, China, in 1991. He received the B.Sc. degree in electrical engineering from Changsha University of Science and Technology in 2013. He is currently working toward the Ph.D. degree of electrical engineering in the College of Electrical and Information Engineering, Hunan University, Changsha, China. From 2018 to 2019, he was a Guest Ph.D. Student with the Department of Energy Technology, Aalborg University, Aalborg, Denmark.

His research interests include the control of hybrid AC/DC power system and the application of distributed energy storages.

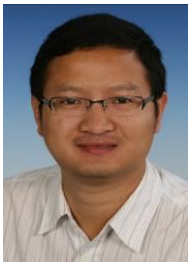

Yong Li (S'09–M'12–SM'14) was born in Henan, China, in 1982. He received the B.Sc. and Ph.D. degrees in 2004 and 2011, respectively, from the College of Electrical and Information Engineering, Hunan University, Changsha, China.

Since 2009, he worked as a Research Associate at the Institute of Energy Systems, Energy Efficiency, and Energy Economics (ie^3), TU Dortmund University, Dortmund, Germany, where he received the second Ph. D. degree in June 2012. After then, he was a Research Fellow with The University of Queensland, Brisbane, Australia. Since 2014, he is a Full Professor of electrical engineering with Hunan University. His current research interests include power system stability analysis and control, ac/dc energy conversion systems and equipment, analysis and control of power quality, and HVDC and FACTS technologies.

Josep M. Guerrero (S'01-M'04-SM'08-F'15) received the B.S. degree in telecommunications engineering, the M.S. degree in electronics engineering, and the Ph.D. degree in power electronics from the Technical University of Catalonia, Barcelona, in 1997, 2000 and 2003,respectively. Since 2011, he has been a Full Professor with the Department of Energy Technology, Aalborg University, Denmark, where he is responsible for the Microgrid Research Program (www.microgrids.et.aau.dk). From 2012 he is a guest Professor at the Chinese Academy of Science and the Nanjing University of Aeronautics and Astronautics; from 2014 he is chair Professor in Shandong University; from 2015 he is a distinguished guest Professor in Hunan University; and from 2016 he is a visiting professor fellow at Aston University, UK, and a guest Professor at the Nanjing University of Posts and Telecommunications. His research interests is oriented to different microgrid aspects, including power electronics, distributed energy-storage systems, hierarchical and cooperative control, energy management systems, smart metering and the internet of things for AC/DC microgrid clusters and islanded minigrids; recently specially focused on maritime microgrids for electrical ships, vessels, ferries and seaports.

Yijia Cao (M'98-SM'13**)** was born in Hunan, China, in 1969. He graduated from Xi'an Jiaotong University, Xi'an, China in 1988 and received M.Sc. degree from Huazhong University of Science and Technology (HUST), Wuhan, China in 1991 and Ph.D from HUST in 1994. From September 1994 to April 2000, he worked as a visiting research fellow, research fellow at Loughborough University, Liverpool University and University of the West England, UK. From 2000 to 2001, he was employed as a full professor of HUST, and from 2001 to 2008, he was employed as a full professor of Zhejiang University, China. He was appointed deputy dean of college of Electrical Engineering, Zhejiang University in 2005. Currently, he is a full professor and vice president of Hunan University, Changsha, China.

His research interests are power system stability control and the application of intelligent systems in power systems.